

Towards Unsupervised Training of Matching-based Graph Edit Distance Solver via Preference-aware GAN

Wei Huang

University of New South Wales
Australia
w.c.huang@unsw.edu.au

Hanchen Wang

University of Technology Sydney
Australia
Hanchen.Wang@uts.edu.au

Dong Wen

University of New South Wales
Australia
dong.wen@unsw.edu.au

Shaozhen Ma

University of New South Wales
Australia
shaozhen.ma@unsw.edu.au

Wenjie Zhang

University of New South Wales
Australia
wenjie.zhang@unsw.edu.au

Xuemin Lin

Shanghai Jiaotong University
China
xuemin.lin@sjtu.edu.cn

Abstract

Graph Edit Distance (GED) is a fundamental graph similarity metric widely used in various applications. However, computing GED is an NP-hard problem. Recent state-of-the-art hybrid GED solver has shown promising performance by formulating GED as a bipartite graph matching problem, then leveraging a generative diffusion model to predict node matching between two graphs, from which both the GED and its corresponding edit path can be extracted using a traditional algorithm. However, such methods typically rely heavily on ground-truth supervision, where the ground-truth labels are often costly to obtain in real-world scenarios. In this paper, we propose GEDRanker, a novel unsupervised GAN-based framework for GED computation. Specifically, GEDRanker consists of a matching-based GED solver and introduces an interpretable preference-aware discriminator with an effective training strategy to guide the matching-based GED solver toward generating high-quality node matching without the need for ground-truth labels. Extensive experiments on benchmark datasets demonstrate that our GEDRanker enables the matching-based GED solver to achieve near-optimal solution quality without any ground-truth supervision.

1 Introduction

Graph Edit Distance (GED) is a widely used graph similarity metric [1, 2, 3] that determines the minimum number of edit operations required to transform one graph into another. It has broad applications in domains such as pattern recognition [4, 5] and computer vision [6, 7]. Figure 1(a) illustrates an example of an optimal edit path for transforming G_1 to G_2 with $\text{GED}(G_1, G_2) = 4$. GED is particularly appealing due to its interpretability and its ability to capture both attribute-level and structural-level similarities between graphs. Traditional exact approaches for computing GED rely on A* search [8, 9, 10]. However, due to the NP-hardness of GED computation, these methods fail to scale to graphs with more than 16 nodes [9], making them impractical for large graphs.

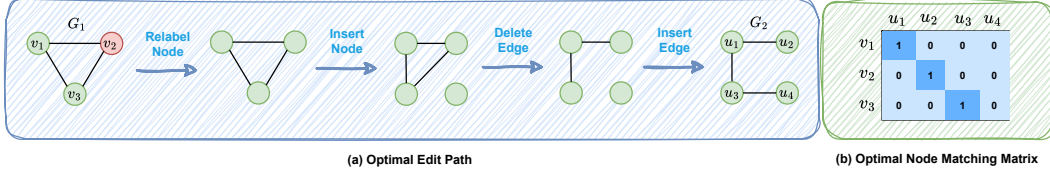


Figure 1: (a) An optimal edit path for converting G_1 to G_2 with $\text{GED}(G_1, G_2) = 4$. (b) An optimal node matching matrix from which an optimal edit path can be derived.

To address the limitations of traditional algorithms, hybrid approaches that combine deep learning with traditional algorithms have been widely explored. Recent hybrid approaches have focused on reformulating GED as a bipartite graph matching problem. Specifically, GEDGNN [11] and GEDIOT [12] propose to train a node matching model that predicts a single node matching probability matrix, where top- k edit paths can be extracted sequentially from the predicted matrices using a traditional algorithm. Later on, the current state-of-the-art GED solver, DiffGED [13], employs a generative diffusion model to predict top- k high quality node matching probability matrices in parallel, which parallelized the extraction of top- k edit paths. Notably, DiffGED has achieved near-optimal solution quality, closely approximating the ground-truth GED with a remarkable computational efficiency. Unfortunately, all existing hybrid GED solvers heavily rely on supervised learning, requiring ground-truth node matching matrices and GED values, which are often infeasible to obtain in practice due to the NP-hard nature of GED computation.

This limits the usability of existing GED methods in real-world scenarios. Therefore, developing an unsupervised training framework for GED solvers is crucial for enhancing real-world applicability. Despite its importance, this direction remains largely underexplored.

In this paper, we propose GEDRanker, a novel GAN-based framework that enables the unsupervised training of a matching-based GED solver without relying on ground-truth node matching matrices. Unlike existing unsupervised training techniques commonly used in other problems, such as REINFORCE [14], GEDRanker provides a more effective and interpretable learning objective (*i.e.*, loss function) that enables GED solver to directly optimize a GED-related score. Specifically, we design an efficient unsupervised training strategy that incorporates a preference-aware discriminator. Rather than directly estimating the resulting edit path length of the node matching matrix, our preference-aware discriminator evaluates the preference over different node matching matrices, thereby providing richer feedback to guide the matching-based GED solver toward exploring high-quality solutions.

Contributions. To the best of our knowledge, GEDRanker is the first unsupervised learning framework for GED computation, providing a scalable and label-free alternative to supervised methods. Experimental results on benchmark datasets show that the current state-of-the-art supervised matching-based GED solver, when trained under our unsupervised framework, achieves near-optimal solution quality comparable to supervised training with the same number of epochs, and outperforms all other supervised learning methods and traditional GED solvers.

2 Related Work

Traditional Approaches. Early approaches for solving GED are primarily based on exact combinatorial algorithms, such as A* search with handcrafted heuristics [9, 10]. While effective on small graphs, these methods are computationally prohibitive on larger graphs due to the NP-hardness of GED computation. To improve scalability, various approximate methods have been developed. These include bipartite matching formulations solved by the Hungarian algorithm [15] or the Volgenant-Jonker algorithm [16], as well as heuristic variants like A*-beam search [8] that limits the search space to enhance efficiency. However, such approximations often suffer from poor solution quality.

Deep Learning Approaches. More recently, deep learning methods have emerged as promising alternatives. SimGNN [17] and its successors [18, 19, 20, 21, 22, 23] formulate GED estimation as a regression task, enabling fast prediction of GED values. However, these methods do not recover the edit path, which is often critical in real applications. As a result, the predicted GED can be smaller than the true value, leading to infeasible solutions for which no valid edit path exists.

Hybrid Approaches. To address the limitations of regression-based deep learning methods, hybrid frameworks have been extensively studied to jointly estimate GED and recover the corresponding edit path. A class of approaches, including Noah [24], GENN-A* [25], and MATA* [26], integrate GNNs with A* search by generating dynamic heuristics or candidate matches. However, these methods still inherit the scalability bottlenecks of A*-based search. To improve both solution quality and computational efficiency, GEDGNN [11] and GEDIOT [12] reformulate GED estimation as a bipartite node matching problem. In this setting, a node matching model is trained to predict a node matching probability matrix, from which top- k edit paths are sequentially extracted using traditional algorithms. To further enhance solution quality and enable parallel extraction of top- k candidates, DiffGED [13], employs a generative diffusion-based node matching model to predict top- k node matching matrices in parallel, achieving near-optimal accuracy with significantly reduced running time. Motivated by its effectiveness and efficiency, we adopt the current state-of-the-art diffusion-based node matching model as the base GED solver of our unsupervised training framework.

3 Preliminaries

3.1 Problem Formulation

Problem Definition (Graph Edit Distance Computation). Given two graphs $G_1 = (V_1, E_1, L_1)$ and $G_2 = (V_2, E_2, L_2)$, where V , E and L represent the node set, edge set, and labeling function, respectively, we consider three types of edit operations: (1) Node insertion or deletion; (2) Edge insertion or deletion; (3) Node relabeling. An edit path is defined as a sequence of edit operations that transforms G_1 into G_2 . The Graph Edit Distance (GED) is the length of the optimal edit path that requires the minimum number of edit operations. In this paper, we aim not only to predict GED, but also to recover the corresponding edit path for the predicted GED.

Edit Path Generation. Given a pair of graphs G_1 and G_2 (assuming $|V_1| \leq |V_2|$), let $\pi \in \{0, 1\}^{|V_1| \times |V_2|}$ denote a binary node matching matrix that satisfy the following constraint:

$$\sum_{u=1}^{|V_2|} \pi[v][u] = 1 \quad \forall v \in V_1, \quad \sum_{v=1}^{|V_1|} \pi[v][u] \leq 1 \quad \forall u \in V_2 \quad (1)$$

where $\pi[v][u] = 1$ if node $v \in V_1$ is matched to node $u \in V_2$; otherwise $\pi[v][u] = 0$. Each $v \in V_1$ matches to exactly one $u \in V_2$, and each $u \in V_2$ matches to at most one $v \in V_1$. Given π , an edit path can be derived with a linear time complexity of $O(|V_2| + |E_1| + |E_2|)$ as follows:

- (1) For each node $u \in V_2$, if u is matched to a node $v \in V_1$ and $L_1(v) \neq L_2(u)$, then relabel $L_1(v)$ to $L_2(u)$. If u is not matched to any node, then insert a new node with label $L_2(u)$ into V_1 , and match it to u . The overall time complexity of this step is $O(|V_2|)$.
- (2) Suppose $v, v' \in V_1$ are matched to $u, u' \in V_2$, respectively. If $(v, v') \in E_1$ but $(u, u') \notin E_2$, then delete (v, v') from E_1 . If $(u, u') \in E_2$ but $(v, v') \notin E_1$, then insert (v, v') into E_1 . The overall time complexity of this step is $O(|E_1| + |E_2|)$.

Figure 1(b) shows an optimal node matching matrix from which the optimal edit path in Figure 1(a) is derived. Thus, computing GED can be reformulated as finding the optimal node matching matrix π^* that minimizes the total number of edit operations $c(G_1, G_2, \pi^*)$ in the resulting edit path.

Greedy Node Matching Matrix Decoding. Let $\hat{\pi} \in [0, 1]^{|V_1| \times |V_2|}$ be a node matching probability matrix, where $\hat{\pi}[v][u]$ denotes the matching probability between node v with node u . A binary node matching matrix π can be greedily decoded from $\hat{\pi}$ with a time complexity of $O(|V_1|^2 |V_2|)$ as follows:

- (1) Select node pair (v, u) with the highest probability in $\hat{\pi}$, and set $\pi[v][u] = 1$.
- (2) Set all values in the v -th row and u -th column of $\hat{\pi}$ to $-\infty$.
- (3) Repeat steps (1) and (2) for $|V_1|$ iterations.

Therefore, GED can be estimated by training a node matching model to generate node matching probability matrix that, when decoded, yields a node matching matrix minimizing the edit path length.

3.2 Supervised Diffusion-based Node Matching Model

The supervised diffusion-based node matching model [13] consists of a forward process and a reverse process. Intuitively, the forward process progressively corrupts the ground-truth node matching matrix π^* over T time steps to create a sequence of increasing noisy latent variables, such that $q(\pi^{1:T}|\pi^0) = \prod_{t=1}^T q(\pi^t|\pi^{t-1})$ with $\pi^0 = \pi^*$, where π^t with $t > 0$ is the noisy node matching matrix that does not need to satisfy the constraint defined in Equation 1. Next, a denoising network g_ϕ takes as input a graph pair (G_1, G_2) , a noisy matching matrix π^t , and the corresponding time step t , is trained to reconstruct π^* from π^t . During inference, the reverse process begins from a randomly sampled noisy matrix π^{t_S} , and iteratively applies g_ϕ to refine it towards a high-quality node matching matrix over a sequence of time steps $\{t_0, t_1, \dots, t_S\}$ with $S \leq T$, $t_0 = 0$ and $t_S = T$, such that $p_\theta(\pi^{t_0:t_S}|G_1, G_2) = p(\pi^{t_S}) \prod_{i=1}^S p_\theta(\pi^{t_{i-1}}|\pi^{t_i}, G_1, G_2)$.

Forward Process. Specifically, let $\tilde{\pi} \in \{0, 1\}^{|V_1| \times |V_2| \times 2}$ denote the one-hot encoding of a node matching matrix $\pi \in \{0, 1\}^{|V_1| \times |V_2|}$. The forward process corrupts π^{t-1} to π^t as: $q(\pi^t|\pi^{t-1}) = \text{Cat}(\pi^t|p = \tilde{\pi}^{t-1}Q_t)$, where $Q_t = \begin{bmatrix} 1 - \beta_t & \beta_t \\ \beta_t & 1 - \beta_t \end{bmatrix}$ is the transition probability matrix, Cat is the categorical distribution and β_t denotes the corruption ratio. The t -step marginal can be written as: $q(\pi^t|\pi^0) = \text{Cat}(\pi^t|p = \tilde{\pi}^0\bar{Q}_t)$, where $\bar{Q}_t = Q_1Q_2\dots Q_t$, this allows π^t to be sampled efficiently from π^0 during training.

Reverse Process. Starting from a randomly sampled noisy node matching matrix π^{t_S} , each step of the reverse process denoises π^{t_i} to $\pi^{t_{i-1}}$ as follows:

$$\begin{aligned} q(\pi^{t_{i-1}}|\pi^{t_i}, \pi^0) &= \frac{q(\pi^{t_i}|\pi^{t_{i-1}}, \pi^0)q(\pi^{t_{i-1}}|\pi^0)}{q(\pi^{t_i}|\pi^0)} \\ p_\phi(\tilde{\pi}^0|\pi^{t_i}, G_1, G_2) &= \sigma(g_\phi(G_1, G_2, \pi^{t_i}, t_i)) \\ p_\phi(\pi^{t_{i-1}}|\pi^{t_i}, G_1, G_2) &= \sum_{\tilde{\pi}} q(\pi^{t_{i-1}}|\pi^{t_i}, \tilde{\pi}^0)p_\phi(\tilde{\pi}^0|\pi^{t_i}, G_1, G_2) \\ \pi^{t_{i-1}} &\sim p_\phi(\pi^{t_{i-1}}|\pi^{t_i}, G_1, G_2) \end{aligned} \quad (2)$$

where $q(\pi^{t_{i-1}}|\pi^{t_i}, \pi^0)$ is the posterior, σ is the Sigmoid activation, and $p_\phi(\tilde{\pi}^0|\pi^{t_i}, G, G')$ is the node matching probabilities predicted by g_ϕ , the detailed architecture of g_ϕ is described in Appendix A.3.

During inference, for each reverse step except the final step, a binary noisy node matching matrix $\pi^{t_{i-1}}$ is sampled from $p_\phi(\pi^{t_{i-1}}|\pi^{t_i}, G_1, G_2)$ via Bernoulli sampling. For the final reverse step, we decode $p_\phi(\pi^0|\pi^{t_1}, G_1, G_2)$ following the greedy method described in Section 3.1 to obtain a constrained binary node matching matrix π^0 . The detailed procedure of reverse process can be found in Appendix A.1. To enhance the solution quality, k random initial π^{t_S} could be sampled in parallel, and k independent reverse processes could be performed in parallel to generate k candidate node matching matrices, the one results in the shortest edit path will be the final solution.

Supervised Training Strategy. In the supervised learning setting, at each training step, given a pair of graphs, a random time step t is sampled, and a noisy matching matrix π^t is sampled from $q(\pi^t|\pi^0)$, where $\pi^0 = \pi^*$ is the ground-truth optimal node matching matrix. The denoising network g_ϕ then takes as input a graph pair (G_1, G_2) , a noisy matching matrix π^t , and the time step t , and is trained to recover π^* from π^t by minimizing:

$$\mathcal{L}_{rec}(\pi^*) = \frac{1}{|V_1||V_2|} \sum_{v=1}^{|V_1|} \sum_{u=1}^{|V_2|} (\pi^*[v][u] \log(\hat{\pi}_{g_\phi}[v][u]) + (1 - \pi^*[v][u]) \log(1 - \sigma(\hat{\pi}_{g_\phi}[v][u]))) \quad (3)$$

where $\hat{\pi}_{g_\phi}$ is the node matching probability matrix such that: $\hat{\pi}_{g_\phi} = \sigma(g_\phi(G_1, G_2, \pi^t, t))$. However, this training strategy heavily relies on pre-computation of the ground-truth node matching matrix.

4 Proposed Approach: GEDRanker

4.1 Unsupervised Training Strategy

In practice, the ground-truth π^* is often unavailable, making it impractical to directly apply the supervised training strategy. A modified training strategy is to store a randomly initialized binary

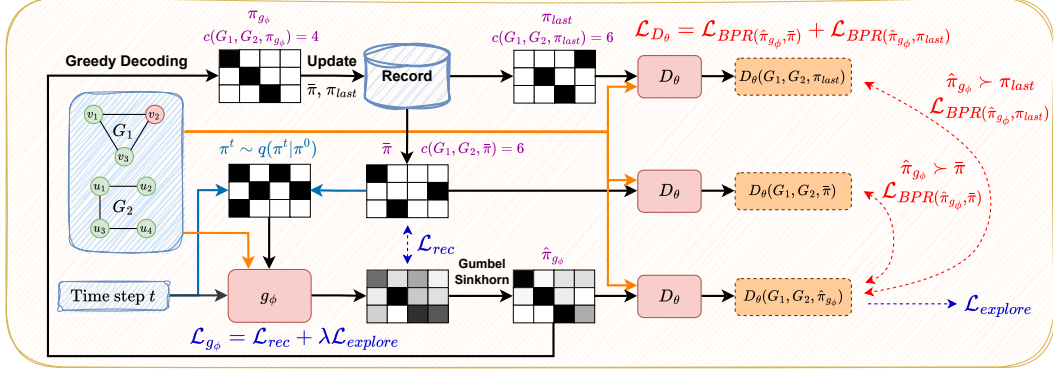


Figure 2: An overview of GEDRanker. For each training step, given a pair of training graphs, we maintain a record of the current best node matching matrix $\bar{\pi}$ and the node matching matrix obtained from the previous training step π_{last} . A noisy matching π^t is sampled at a random diffusion time step t and denoised by the denoising network g_ϕ to produce node matching scores. The resulting matching probability matrix $\hat{\pi}_{g_\phi}$ is obtained via Gumbel-Sinkhorn and greedily decoded to π_{g_ϕ} . The preference-aware discriminator D_θ is trained to rank the preference over $\bar{\pi}$, π_{last} , and $\hat{\pi}_{g_\phi}$. Next, g_ϕ is trained to recover $\bar{\pi}$ and maximize the preference score $D_\theta(G_1, G_2, \pi_{g_\phi})$. Finally, the record is updated by π_{g_ϕ} .

constrained node matching matrix as the current best solution $\bar{\pi}$ for each training graph pair. At each training step, for a given pair of graphs, we sample a random t , and sample a noisy matching matrix π^t from $q(\pi^t | \pi^0)$, with $\pi^0 = \bar{\pi}$, then g_ϕ is trained to recover $\bar{\pi}$ from π^t by minimizing $\mathcal{L}_{rec}(\bar{\pi})$. If the node matching matrix π_{g_ϕ} decoded from $\hat{\pi}_{g_\phi} = \sigma(g_\phi(G_1, G_2, \pi^t, t))$ yields a shorter edit path (i.e., $c(G_1, G_2, \pi_{g_\phi}) < c(G_1, G_2, \bar{\pi})$), then $\bar{\pi}$ is updated to π_{g_ϕ} . This guarantees that g_ϕ progressively finds a better solution during training, while recovering the current best solution.

However, the training objective in the above approach is fundamentally exploitative, as it only focused on recovering the currently best solution rather than actively exploring alternative solutions. While exploitation is beneficial in later stages when a high-quality solution is available, it is inefficient in the early stages of training, where the current best solution is likely far from optimal. In such cases, blindly recovering a suboptimal node matching matrix is ineffective and can mislead g_ϕ into poor learning directions, and hinder its ability to explore better solutions. Therefore, an effective training objective should prioritize exploring for better solutions in the early stages and shift its focus toward recovering high-quality solutions in the later stages.

RL-based Training Objective. A widely adopted strategy for guiding g_ϕ 's exploration towards better solutions is the use of reinforcement learning, specifically the REINFORCE [14], such that:

$$\nabla_\phi J(\phi) = \mathbb{E}_{\pi_{g_\phi}} [(c(G_1, G_2, \pi_{g_\phi}) - b) \nabla_\phi \log \sigma(g_\phi(G_1, G_2, \pi^t, t))] \quad (4)$$

where b is a baseline used to reduce gradient variance. This method adjusts the parameters of g_ϕ to increase or decrease the matching probability of each node pair based on the resulting edit path length, encouraging the model to generate node matching probability matrices that are more likely to yield shorter edit paths.

Unfortunately, this approach suffers from several limitations: (1) It does not directly optimize the graph edit distance and lacks interpretability, as the edit path length only serves as a scale for gradient updates; (2) It assumes all node pairs in π_{g_ϕ} contribute equally to the edit path length, thus all node pairs are assigned with the same scale, making it difficult to distinguish correctly predicted node matching probabilities from incorrect ones; (3) It ignores the combinatorial dependencies among node pairs, but the generated edit path is highly sensitive to such dependencies, limiting g_ϕ 's ability to efficiently explore high quality solutions.

GAN-based Training Objective. To overcome the limitations of REINFORCE, our GAN-based framework, GEDRanker, leverages a discriminator D_θ to guide g_ϕ 's exploration for better solutions. Specifically, given a node matching matrix π , the discriminator D_θ is trained to evaluate π and assign a GED-related score $D_\theta(G_1, G_2, \pi)$. If π corresponds to a shorter edit path, then it will be assigned with a higher score; otherwise, a lower score. Therefore, g_ϕ is trained to maximize $D_\theta(G_1, G_2, \pi_{g_\phi})$.

Preference-aware Training Objective. To ensure that D_θ learns the correct preference, we introduce a preference-aware discriminator. A node matching matrix with a shorter edit path should be preferred (\succ) over one with a longer edit path. The objective of the preference-aware discriminator is to guarantee that the score assigned to the preferred node matching matrix is ranked higher than that of the less preferred one. Specifically, at each training step, given a pair of graphs, we have the current best node matching matrix $\bar{\pi}$ and the predicted node matching probability matrix $\hat{\pi}_{g_\phi} = S(g_\phi(G_1, G_2, \pi^t, t))$. The preference-aware discriminator is trained to minimize the following Bayes Personalized Ranking (BPR) loss [28]:

$$\mathcal{L}_{BPR(\hat{\pi}_{g_\phi}, \bar{\pi})} = \begin{cases} -\log \sigma(D_\theta(G_1, G_2, \hat{\pi}_{g_\phi}) - D_\theta(G_1, G_2, \bar{\pi})) & \text{if } c(G_1, G_2, \pi_{g_\phi}) \leq c(G_1, G_2, \bar{\pi}) \\ -\log \sigma(D_\theta(G_1, G_2, \bar{\pi}) - D_\theta(G_1, G_2, \hat{\pi}_{g_\phi})) & \text{if } c(G_1, G_2, \pi_{g_\phi}) \geq c(G_1, G_2, \bar{\pi}) \end{cases} \quad (8)$$

BPR encourages the preference-aware discriminator to increase the preference score of the better node matching matrix while simultaneously decreasing the preference score of the worse one, thereby promoting a clear separation between high and low quality solutions. Note that, other ranking loss functions, such as Hinge Loss, could be an alternative. Now, Case 1 yields a lower loss of $\mathcal{L}_{BPR(\pi_1, \pi_2)} = 0.3711$, whereas Case 2 results in a higher loss of $\mathcal{L}_{BPR(\pi_1, \pi_2)} = 0.7981$. Consequently, D_θ would choose Case 1, and g_ϕ would be encouraged to generate π_2 over π_1 . Notably, for the special case where $c(G_1, G_2, \pi_{g_\phi}) = c(G_1, G_2, \bar{\pi})$, $\mathcal{L}_{BPR(\hat{\pi}_{g_\phi}, \bar{\pi})}$ is computed in both directions to ensure that the loss is minimized only if $\hat{\pi}_{g_\phi}$ and $\bar{\pi}$ are assigned with the same preference score.

Moreover, finding a better solution becomes increasingly challenging as training progresses. Consequently, $\bar{\pi}$ is updated less frequently in later training stages, leading to a scenario where a single node matching matrix may dominate $\bar{\pi}$. In this case, the discriminator can only learn to rank $\hat{\pi}_{g_\phi}$ against this specific $\bar{\pi}$, but may fail to correctly rank $\hat{\pi}_{g_\phi}$ against other node matching matrices. To deal with such case, we store an additional historical node matching matrix π_{last} decoded from $\hat{\pi}_{g_\phi}$ in the previous training step. We then compute an additional ranking loss $\mathcal{L}_{BPR(\hat{\pi}_{g_\phi}, \pi_{\text{last}})}$ to encourage a more robust ranking mechanism. Overall, the discriminator is trained to minimize the following loss:

$$\mathcal{L}_{D_\theta} = \mathcal{L}_{BPR(\hat{\pi}_{g_\phi}, \bar{\pi})} + \mathcal{L}_{BPR(\hat{\pi}_{g_\phi}, \pi_{\text{last}})} \quad (9)$$

The overall framework of GEDRanker is illustrated in Figure 2 and outlined in Algorithm 3.

Discriminator Architecture. To effectively capture the dependencies among node pairs and distinguish the influence of each predicted node matching on the resulting edit path, our D_θ leverages GIN [29] and Anisotropic Graph Neural Network (AGNN) [30, 31, 32] to compute the embeddings of each node pair, then estimates the preference score directly based on these embeddings. Due to the space limitation, more details about the architecture of D_θ can be found in Appendix A.3 and C.3.

5 Experiments

5.1 Experimental Settings

Datasets. We conduct experiments on three widely used real world datasets: AIDS700 [17], Linux [33, 17], and IMDB [17, 34]. Each dataset is split into 60%, 20% and 20% as training graphs, validation graphs and testing graphs, respectively. We construct training, validation, and testing graph pairs, and generate their corresponding ground-truth GEDs and node matching matrices following the strategy described in [11]. More details of the datasets can be found in Appendix B.1.

Baselines. We categorize baseline methods and our GEDRanker into three groups: (1) Traditional approximation methods: Hungarian [15], VJ [16] and GEDGW [12]; (2) Supervised hybrid methods: Noah [24], GENN-A* [25], MATA* [26], GEDGNN [11], GEDIOT [12] and DiffGED [13]; (3) Unsupervised hybrid method: GEDRanker. Due to the space limitations, the implementation details of our GEDRanker could be found in Appendix B.2.

Evaluation Metrics. We evaluate the performance of each model using the following metrics: (1) *Mean Absolute Error* (MAE) measures average absolute error between the predicted GED and the ground-truth GED; (2) *Accuracy* measures the proportion of test pairs whose predicted GED equals the ground-truth GED; (3) *Spearman’s Rank Correlation Coefficient* (ρ), and (4) *Kendall’s Rank Correlation Coefficient* (τ) both measure the matching ratio between the ranking results of

Table 1: Overall performance on testing graph pairs. Methods with a running time exceeding 24 hours are marked with -. \uparrow : higher is better. \downarrow : lower is better. **Bold**: best in its own group. Trad, SL and UL denotes Traditional, Supervised Learning and Unsupervised Learning, respectively. Results for baselines, except for GEDIOT and GEDGW, are taken from [13].

Datasets	Models	Type	MAE \downarrow	Accuracy \uparrow	ρ \uparrow	τ \uparrow	$p@10$ \uparrow	$p@20$ \uparrow	Time(s) \downarrow
AIDS700	Hungarian	Trad	8.247	1.1%	0.547	0.431	52.8%	59.9%	0.00011
	VJ	Trad	14.085	0.6%	0.372	0.284	41.9%	52%	0.00017
	GEDGW	Trad	0.811	53.9%	0.866	0.78	84.9%	85.7%	0.39255
	Noah	SL	3.057	6.6%	0.751	0.629	74.1%	76.9%	0.6158
	GENN-A*	SL	0.632	61.5%	0.903	0.815	85.6%	88%	2.98919
	MATA*	SL	0.838	58.7%	0.8	0.718	73.6%	77.6%	0.00487
	GEDGNN	SL	1.098	52.5%	0.845	0.752	89.1%	88.3%	0.39448
	GEDIOT	SL	1.188	53.5%	0.825	0.73	88.6%	86.7%	0.39357
	DiffGED	SL	0.022	98%	0.996	0.992	99.8%	99.7%	0.0763
	GEDRanker (Ours)	UL	0.088	92.6%	0.984	0.969	99.1%	99.1%	0.0759
Linux	Hungarian	Trad	5.35	7.4%	0.696	0.605	74.8%	79.6%	0.00009
	VJ	Trad	11.123	0.4%	0.594	0.5	72.8%	76%	0.00013
	GEDGW	Trad	0.532	75.4%	0.919	0.864	90.5%	92.2%	0.1826
	Noah	SL	1.596	9%	0.9	0.834	92.6%	96%	0.24457
	GENN-A*	SL	0.213	89.4%	0.954	0.905	99.1%	98.1%	0.68176
	MATA*	SL	0.18	92.3%	0.937	0.893	88.5%	91.8%	0.00464
	GEDGNN	SL	0.094	96.6%	0.979	0.969	98.9%	99.3%	0.12863
	GEDIOT	SL	0.117	95.3%	0.978	0.966	98.8%	99%	0.13535
	DiffGED	SL	0.0	100%	1.0	1.0	100%	100%	0.06982
	GEDRanker (Ours)	UL	0.01	99.5%	0.997	0.995	100%	99.8%	0.06973
IMDB	Hungarian	Trad	21.673	45.1%	0.778	0.716	83.8%	81.9%	0.0001
	VJ	Trad	44.078	26.5%	0.4	0.359	60.1%	62%	0.00038
	GEDGW	Trad	0.349	93.9%	0.966	0.953	99.1%	98.3%	0.37496
	Noah	SL	-	-	-	-	-	-	-
	GENN-A*	SL	-	-	-	-	-	-	-
	MATA*	SL	-	-	-	-	-	-	-
	GEDGNN	SL	2.469	85.5%	0.898	0.879	92.4%	92.1%	0.42428
	GEDIOT	SL	2.822	84.5%	0.9	0.878	92.3%	92.7%	0.41959
	DiffGED	SL	0.937	94.6%	0.982	0.973	97.5%	98.3%	0.15105
	GEDRanker (Ours)	UL	1.019	94%	0.999	0.97	96.1%	97%	0.15111

the predicted GED and the ground-truth GED for each query test graph; (5) *Precision at 10/20* ($p@10$, $p@20$) measures the proportion of predicted top-10/20 most similar graphs that appear in the ground-truth top-10/20 similar graphs for each query test graph. (6) *Time (s)* measures the average running time of each test graph pair.

5.2 Main Results

Table 1 presents the overall performance of each method on the test graph pairs. Among supervised methods, the diffusion-based node matching model DiffGED achieves near-optimal accuracy across all datasets. Our unsupervised GEDRanker, which trains diffusion-based node matching model without ground-truth labels but with the same number of training epochs, also outperforms other supervised methods and achieves near-optimal solution quality, with an insignificant performance gap compared to DiffGED.

Furthermore, compared to the traditional approximation method GEDGW, GEDRanker consistently achieves higher solution quality while maintaining shorter running times across all datasets. It is worth noting that on the IMDB dataset, GEDGW exhibits a lower MAE, this is because IMDB contains synthetic large graph pairs, where approximated ground-truth GED values might be higher than the actual ground-truth GED values. As a result, a lower MAE only reflects the predicted GED values are close to the approximated ground-truth values.

5.3 Ablation Study

Exploration Ability. To evaluate the significant of the exploration during unsupervised learning as well as the exploration ability of our proposed GEDRanker, we create three variant models: (1) *GEDRanker (plain)*, which simply trains g_ϕ only to recover the current best solution using $\mathcal{L}_{rec}(\bar{\pi})$ without any exploration; (2) *GEDRanker (RL)*, which guides g_ϕ 's exploration using REINFORCE by replacing $\mathcal{L}_{explore}$ with Equation 4; (3) *GEDRanker (GED)*, which replaces the preference-aware discriminator with a discriminator that directly estimates the edit path length (Equation 7).

Table 2 presents the performance of each variant model on testing graph pairs. The results show that the performance of GEDRanker (plain) drops significantly without exploration, indicating that a purely exploitative approach focused solely on recovering the current best solution is insufficient. Furthermore, Figure 3 shows the average edit path length of the best found solutions on training graph pairs. Obviously, GEDRanker (plain) exhibits the weakest ability to discover better solutions, which misleads g_ϕ into recovering suboptimal solutions.

Table 2: Ablation study.

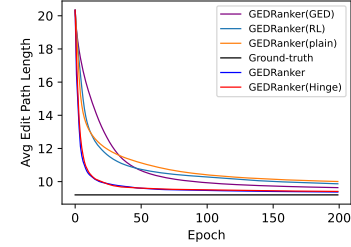
Datasets	Models	MAE ↓	Accuracy ↑	ρ ↑	τ ↑	$p@10$ ↑	$p@20$ ↑
AIDS700	GEDRanker (plain)	0.549	65.4%	0.905	0.837	91.7%	91.5%
	GEDRanker (RL)	0.458	69.3%	0.921	0.86	91.1%	92.7%
	GEDRanker (GED)	0.237	82.3%	0.956	0.919	97.6%	96.5%
	GEDRanker (Hinge)	0.114	90.5%	0.98	0.96	98.9%	98.6%
	GEDRanker	0.088	92.6%	0.984	0.969	99.1%	99.1%
Linux	GEDRanker (plain)	0.079	96.2%	0.984	0.973	98.1%	98.3%
	GEDRanker (RL)	0.04	98%	0.99	0.984	99.2%	99.2%
	GEDRanker (GED)	0.017	99.2%	0.995	0.992	99.4%	99.6%
	GEDRanker (Hinge)	0.002	99.9%	0.999	0.999	100%	100%
	GEDRanker	0.01	99.5%	0.997	0.995	100%	99.8%

For the variant models that incorporate exploration, GEDRanker (RL), which guides the exploration of g_ϕ using REINFORCE, slightly improves the overall performance and exploration ability compared to GEDRanker (plain) as demonstrated in Table 2 and Figure 3. However, there still remains a significant performance gap compared to our GAN-based approaches GEDRanker and GEDRanker (GED). This gap arises because REINFORCE cannot directly optimize GED and struggles to capture the dependencies among node pairs as well as the individual impact of each node pair on the resulting edit path, whereas our GAN-based framework is able to capture both effectively.

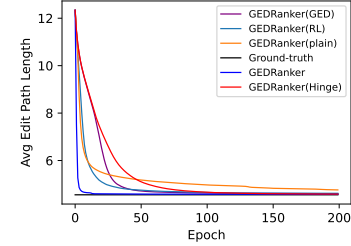
Moreover, the preference-aware discriminator used in GEDRanker further enhances the exploration ability, compared to the discriminator used in GEDRanker (GED) that directly estimates the edit path length. As shown in Figure 3, the average edit path length of the best solution found by GEDRanker converges to a near-optimal value significantly faster than all variant models, indicating a strong ability to explore for high quality solutions. Consequently, this allows g_ϕ more epochs to recover high quality solutions, thereby improving the overall performance, as demonstrated in Table 2.

In contrast, GEDRanker (GED) struggles to identify better solutions during the early training phase. This observation aligns with our earlier analysis: a discriminator that directly estimates edit path length may produce incorrect preferences over different π when D_θ is not yet well-trained, thereby misguiding the exploration direction of g_ϕ . As training progresses, the edit path estimation becomes more accurate, such incorrect preference occurs less frequently, thus its exploration ability becomes better than GEDRanker (plain) and GEDRanker (RL).

Ranking Loss. For the preference-aware discriminator, we adopt the BPR ranking loss. To evaluate the effect of alternative ranking loss, we introduce a variant model, *GEDRanker (Hinge)*, which replaces BPR with a Hinge loss to rank the preference over different node matching matrices π . Following the same setting as in Equation 8, the Hinge loss is computed with a margin of 1 when the two node matching matrices yield different edit path lengths, and with a margin of 0 when they result in the same edit path length. In the latter case, the loss is computed in both directions to encourage their predicted scores to be as similar as possible. The detailed Hinge loss is shown in Appendix A.4.



(a) AIDS700



(b) Linux

Figure 3: Average edit path length of the best found node matching matrices on training graph pairs.

The overall performance of GEDRanker (Hinge) is very close to that of GEDRanker with BPR loss, and both outperform all non-preference-aware variants, as shown in Table 2, further validating the effectiveness of our proposed preference-aware discriminator. However, as shown in Figure 3, the exploration ability of GEDRanker (Hinge) is less stable compared to GEDRanker. On the AIDS700 dataset, they both exhibit similar exploration trends, while on the Linux dataset, GEDRanker (Hinge) performs poorly during the early training phase. This discrepancy arises because Hinge loss produces non-smooth, discontinuous gradients, and it is sensitive to the choice of margin, making optimization less stable. Therefore, we choose to adopt BPR loss for our preference-aware discriminator.

6 Conclusion

In this paper, we propose GEDRanker, the first unsupervised training framework for GED computation. Specifically, GEDRanker adopts a GAN-based design, consisting of a node matching-based GED solver and a preference-aware discriminator that evaluates the relative quality of different node matching matrices. Extensive experiments on benchmark datasets demonstrate that GEDRanker enables the current state-of-the-art supervised GED solver to achieve near-optimal performance under a fully unsupervised setting, while also outperforming all other supervised and traditional baselines.

References

- [1] K. Gouda and M. Arafa, “An improved global lower bound for graph edit similarity search,” *Pattern Recognition Letters*, vol. 58, pp. 8–14, 2015.
- [2] Y. Liang and P. Zhao, “Similarity search in graph databases: A multi-layered indexing approach,” in *2017 IEEE 33rd International Conference on Data Engineering (ICDE)*. IEEE, 2017, pp. 783–794.
- [3] H. Bunke, “On a relation between graph edit distance and maximum common subgraph,” *Pattern recognition letters*, vol. 18, no. 8, pp. 689–694, 1997.
- [4] P. Maergner, V. Pondenkandath, M. Alberti, M. Liwicki, K. Riesen, R. Ingold, and A. Fischer, “Combining graph edit distance and triplet networks for offline signature verification,” *Pattern Recognition Letters*, vol. 125, pp. 527–533, 2019.
- [5] H. Bunke and G. Allermann, “Inexact graph matching for structural pattern recognition,” *Pattern Recognition Letters*, vol. 1, no. 4, pp. 245–253, 1983.
- [6] M. Cho, K. Alahari, and J. Ponce, “Learning graphs to match,” in *Proceedings of the IEEE International Conference on Computer Vision*, 2013, pp. 25–32.
- [7] L. Chen, G. Lin, S. Wang, and Q. Wu, “Graph edit distance reward: Learning to edit scene graph,” in *Computer Vision—ECCV 2020: 16th European Conference, Glasgow, UK, August 23–28, 2020, Proceedings, Part XIX 16*. Springer, 2020, pp. 539–554.
- [8] M. Neuhaus, K. Riesen, and H. Bunke, “Fast suboptimal algorithms for the computation of graph edit distance,” in *Structural, Syntactic, and Statistical Pattern Recognition: Joint IAPR International Workshops, SSPR 2006 and SPR 2006, Hong Kong, China, August 17–19, 2006. Proceedings*. Springer, 2006, pp. 163–172.
- [9] D. B. Blumenthal and J. Gamper, “On the exact computation of the graph edit distance,” *Pattern Recognition Letters*, vol. 134, pp. 46–57, 2020.
- [10] L. Chang, X. Feng, X. Lin, L. Qin, W. Zhang, and D. Ouyang, “Speeding up ged verification for graph similarity search,” in *2020 IEEE 36th International Conference on Data Engineering (ICDE)*. IEEE, 2020, pp. 793–804.
- [11] C. Piao, T. Xu, X. Sun, Y. Rong, K. Zhao, and H. Cheng, “Computing graph edit distance via neural graph matching,” *Proceedings of the VLDB Endowment*, vol. 16, no. 8, pp. 1817–1829, 2023.
- [12] Q. Cheng, D. Yan, T. Wu, Z. Huang, and Q. Zhang, “Computing approximate graph edit distance via optimal transport,” *Proceedings of the ACM on Management of Data*, vol. 3, no. 1, pp. 1–26, 2025.
- [13] W. Huang, H. Wang, D. Wen, W. Zhang, Y. Zhang, and X. Lin, “Diffged: Computing graph edit distance via diffusion-based graph matching,” *arXiv preprint arXiv:2503.18245*, 2025.

- [14] R. J. Williams, “Simple statistical gradient-following algorithms for connectionist reinforcement learning,” *Machine learning*, vol. 8, pp. 229–256, 1992.
- [15] K. Riesen and H. Bunke, “Approximate graph edit distance computation by means of bipartite graph matching,” *Image and Vision computing*, vol. 27, no. 7, pp. 950–959, 2009.
- [16] H. Bunke, K. Riesen, and S. Fankhauser, “Speeding up graph edit distance computation through fast bipartite matching,” 2011.
- [17] Y. Bai, H. Ding, S. Bian, T. Chen, Y. Sun, and W. Wang, “Simgcn: A neural network approach to fast graph similarity computation,” in *Proceedings of the twelfth ACM international conference on web search and data mining*, 2019, pp. 384–392.
- [18] J. Bai and P. Zhao, “Tagsim: Type-aware graph similarity learning and computation,” *Proceedings of the VLDB Endowment*, vol. 15, no. 2, 2021.
- [19] W. Zhuo and G. Tan, “Efficient graph similarity computation with alignment regularization,” *Advances in Neural Information Processing Systems*, vol. 35, pp. 30 181–30 193, 2022.
- [20] X. Ling, L. Wu, S. Wang, T. Ma, F. Xu, A. X. Liu, C. Wu, and S. Ji, “Multilevel graph matching networks for deep graph similarity learning,” *IEEE Transactions on Neural Networks and Learning Systems*, vol. 34, no. 2, pp. 799–813, 2021.
- [21] Y. Bai, H. Ding, K. Gu, Y. Sun, and W. Wang, “Learning-based efficient graph similarity computation via multi-scale convolutional set matching,” in *Proceedings of the AAAI conference on artificial intelligence*, vol. 34, no. 04, 2020, pp. 3219–3226.
- [22] Z. Zhang, J. Bu, M. Ester, Z. Li, C. Yao, Z. Yu, and C. Wang, “H2mn: Graph similarity learning with hierarchical hypergraph matching networks,” in *Proceedings of the 27th ACM SIGKDD conference on knowledge discovery & data mining*, 2021, pp. 2274–2284.
- [23] C. Qin, H. Zhao, L. Wang, H. Wang, Y. Zhang, and Y. Fu, “Slow learning and fast inference: Efficient graph similarity computation via knowledge distillation,” *Advances in Neural Information Processing Systems*, vol. 34, pp. 14 110–14 121, 2021.
- [24] L. Yang and L. Zou, “Noah: Neural-optimized a* search algorithm for graph edit distance computation,” in *2021 IEEE 37th International Conference on Data Engineering (ICDE)*. IEEE, 2021, pp. 576–587.
- [25] R. Wang, T. Zhang, T. Yu, J. Yan, and X. Yang, “Combinatorial learning of graph edit distance via dynamic embedding,” in *Proceedings of the IEEE/CVF Conference on Computer Vision and Pattern Recognition*, 2021, pp. 5241–5250.
- [26] J. Liu, M. Zhou, S. Ma, and L. Pan, “Mata*: Combining learnable node matching with a* algorithm for approximate graph edit distance computation,” in *Proceedings of the 32nd ACM International Conference on Information and Knowledge Management*, 2023, pp. 1503–1512.
- [27] G. Mena, D. Belanger, S. Linderman, and J. Snoek, “Learning latent permutations with gumbel-sinkhorn networks,” *arXiv preprint arXiv:1802.08665*, 2018.
- [28] S. Rendle, C. Freudenthaler, Z. Gantner, and L. Schmidt-Thieme, “Bpr: Bayesian personalized ranking from implicit feedback,” *arXiv preprint arXiv:1205.2618*, 2012.
- [29] K. Xu, W. Hu, J. Leskovec, and S. Jegelka, “How powerful are graph neural networks?” *arXiv preprint arXiv:1810.00826*, 2018.
- [30] C. K. Joshi, Q. Cappart, L.-M. Rousseau, and T. Laurent, “Learning the travelling salesperson problem requires rethinking generalization,” *arXiv preprint arXiv:2006.07054*, 2020.
- [31] Z. Sun and Y. Yang, “Difusco: Graph-based diffusion solvers for combinatorial optimization,” *Advances in Neural Information Processing Systems*, vol. 36, pp. 3706–3731, 2023.
- [32] R. Qiu, Z. Sun, and Y. Yang, “Dimes: A differentiable meta solver for combinatorial optimization problems,” *Advances in Neural Information Processing Systems*, vol. 35, pp. 25 531–25 546, 2022.
- [33] X. Wang, X. Ding, A. K. Tung, S. Ying, and H. Jin, “An efficient graph indexing method,” in *2012 IEEE 28th International Conference on Data Engineering*. IEEE, 2012, pp. 210–221.
- [34] P. Yanardag and S. Vishwanathan, “Deep graph kernels,” in *Proceedings of the 21th ACM SIGKDD international conference on knowledge discovery and data mining*, 2015, pp. 1365–1374.

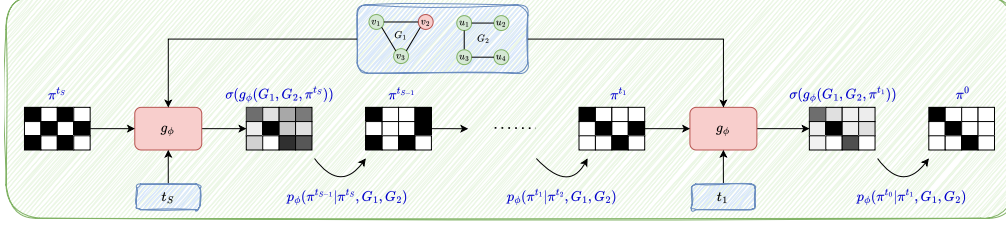


Figure 4: Reverse process of diffusion-based node matching model during inference.

- [35] A. Vaswani, N. Shazeer, N. Parmar, J. Uszkoreit, L. Jones, A. N. Gomez, Ł. Kaiser, and I. Polosukhin, “Attention is all you need,” *Advances in neural information processing systems*, vol. 30, 2017.
- [36] T. Cai, S. Luo, K. Xu, D. He, T.-y. Liu, and L. Wang, “Graphnorm: A principled approach to accelerating graph neural network training,” in *International Conference on Machine Learning*. PMLR, 2021, pp. 1204–1215.

A Detailed Method

Algorithm 2 Reverse Process

Input: A pair of graphs (G_1, G_2) ;
1: $\pi^{t_S} \sim \text{Bernoulli}(0.5)^{|V_1| \times |V_2|}$;
2: **for** $i = S$ to 1 **do**
3: $p_\phi(\tilde{\pi}^0 | \pi^{t_i}, G_1, G_2) \leftarrow \sigma(g_\phi(G_1, G_2, \pi^{t_i}, t_i))$;
4: **if** $i \neq 1$ **then**
5: $\pi^{t_{i-1}} \sim p_\phi(\pi^{t_{i-1}} | \pi^{t_i}, G_1, G_2)$;
6: **else**
7: $\pi^0 \leftarrow \text{Greedy}(p_\phi(\pi^{t_{i-1}} | \pi^{t_i}, G_1, G_2))$;
8: **end if**
9: **end for**
10: **return** π^0 ;

Algorithm 3 GEDRanker Training Strategy

1: Initialize $\bar{\pi} \leftarrow \text{Greedy}(\hat{\pi})$, $\pi_{\text{last}} \leftarrow \text{Greedy}(\hat{\pi})$, with $\hat{\pi} \sim \mathcal{U}(0, 1)^{|V_1| \times |V_2|}$;
2: **for** each epoch **do**
3: Sample $t \sim \mathcal{U}(\{1, \dots, T\})$ and $\pi^t \sim q(\pi^t | \bar{\pi})$;
4: $\hat{\pi}_{g_\phi} \leftarrow S(g_\phi(G_1, G_2, \pi^t, t))$;
5: $\pi_{g_\phi} \leftarrow \text{Greedy}(\hat{\pi}_{g_\phi})$;
6: Compute $D_\theta(G_1, G_2, \hat{\pi}_{g_\phi})$, $D_\theta(G_1, G_2, \bar{\pi})$, $D_\theta(G_1, G_2, \pi_{\text{last}})$;
7: Compute $\mathcal{L}_{\mathcal{D}_\theta}$ and update D_θ ;
8: Compute $D_\theta(G_1, G_2, \hat{\pi}_{g_\phi})$;
9: Compute \mathcal{L}_{g_ϕ} and update g_ϕ ;
10: **if** $c(G_1, G_2, \pi_{g_\phi}) < c(G_1, G_2, \bar{\pi})$ **then**
11: Update $\bar{\pi} \leftarrow \pi_{g_\phi}$;
12: **end if**
13: Update $\pi_{\text{last}} \leftarrow \pi_{g_\phi}$;
14: **end for**

A.1 Diffusion-based Node Matching Model Reverse Process

The detailed reverse process of diffusion-based node matching model is illustrated in Figure 4 and outlined in Algorithm 2.

A.2 GEDRanker

The detailed unsupervised training strategy of GEDRanker is outlined in Algorithm 3.

A.3 Network Architecture

Network Architecture of g_ϕ . The denoising network g_ϕ takes as input a graph pair (G_1, G_2) , a noisy matching matrix π^t , and the corresponding time step t , then predicts a matching score for each node pair. Intuitively, g_ϕ works by computing pair embedding of each node pair, followed by computing the matching score of each node pair based on its pair embedding.

Specifically, for each node $v \in V_1$ and $u \in V_2$, we initialize the node embeddings \mathbf{h}_v^0 and \mathbf{h}_u^0 as the one-hot encoding of their labels $L_1(v)$ and $L_2(u)$, respectively. For each node pair $(v, u) \in \pi^t$, we construct two directional pair embeddings \mathbf{h}_{vu}^0 and \mathbf{h}_{uv}^0 to ensure permutation invariance, since the input graph pair has no inherent order, i.e., $\text{GED}(G_1, G_2) = \text{GED}(G_2, G_1)$. Both \mathbf{h}_{vu}^0 and \mathbf{h}_{uv}^0 are initialized using the sinusoidal embeddings [35] of $\pi^t[v][u]$. Moreover, the time step embedding \mathbf{h}_t is initialized as the sinusoidal embedding of t .

Each layer l of g_ϕ consists of a two stage update. In the first stage, we independently update the node embeddings of each graph based on its own graph structure using siamese GIN [29] as follows:

$$\begin{aligned}\hat{\mathbf{h}}_v^l &= \text{GN}_{G_1}(\text{MLP}((1 + \epsilon^l) \cdot \mathbf{h}_v^{l-1} + \sum_{v' \in \mathcal{N}_{G_1}(v)} \mathbf{h}_{v'}^{l-1})) \\ \hat{\mathbf{h}}_u^l &= \text{GN}_{G_2}(\text{MLP}((1 + \epsilon^l) \cdot \mathbf{h}_u^{l-1} + \sum_{u' \in \mathcal{N}_{G_2}(u)} \mathbf{h}_{u'}^{l-1}))\end{aligned}\quad (10)$$

where ϵ^l is a learnable scalar, MLP denotes a multi-layer perceptron, GN_{G_1} and GN_{G_2} denote graph normalization [36] over G_1 and G_2 , respectively.

In the second stage, we simultaneously update the node embeddings of both graphs and the pair embeddings via Anisotropic Graph Neural Network (AGNN) [30, 31, 32], which incorporates the noisy interactions between node pairs and the corresponding time step t :

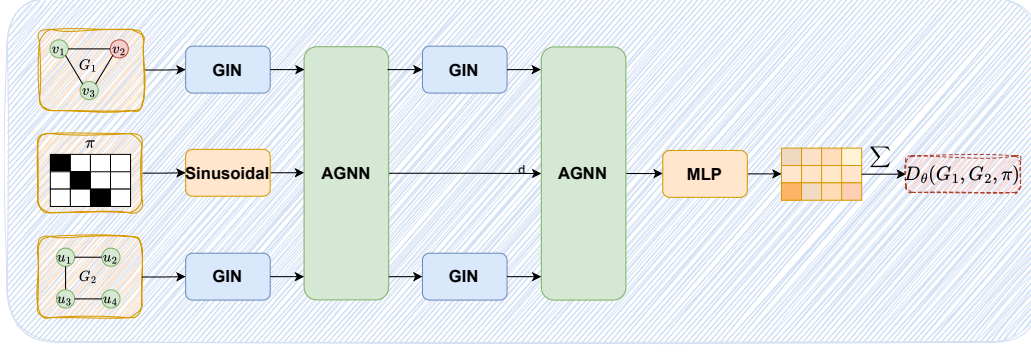
$$\begin{aligned}\hat{\mathbf{h}}_{vu}^l &= \mathbf{W}_1^l \mathbf{h}_{vu}^{l-1}, \quad \hat{\mathbf{h}}_{uv}^l = \mathbf{W}_1^l \mathbf{h}_{uv}^{l-1} \\ \tilde{\mathbf{h}}_{vu}^l &= \mathbf{W}_2^l \hat{\mathbf{h}}_{vu}^l + \mathbf{W}_3^l \hat{\mathbf{h}}_v^l + \mathbf{W}_4^l \hat{\mathbf{h}}_u^l \\ \tilde{\mathbf{h}}_{uv}^l &= \mathbf{W}_2^l \hat{\mathbf{h}}_{uv}^l + \mathbf{W}_3^l \hat{\mathbf{h}}_u^l + \mathbf{W}_4^l \hat{\mathbf{h}}_v^l \\ \mathbf{h}_{vu}^l &= \hat{\mathbf{h}}_{vu}^l + \text{MLP}(\text{ReLU}(\text{GN}_\pi(\tilde{\mathbf{h}}_{vu}^l)) + \mathbf{W}_5^l \mathbf{h}_t) \\ \mathbf{h}_{uv}^l &= \hat{\mathbf{h}}_{uv}^l + \text{MLP}(\text{ReLU}(\text{GN}_\pi(\tilde{\mathbf{h}}_{uv}^l)) + \mathbf{W}_5^l \mathbf{h}_t) \\ \mathbf{h}_v^l &= \hat{\mathbf{h}}_v^l + \text{ReLU}(\text{GN}_{G_1 G_2}(\mathbf{W}_6^l \hat{\mathbf{h}}_v^l + \sum_{u' \in V_2} \mathbf{W}_7^l \hat{\mathbf{h}}_{u'}^l \odot \sigma(\tilde{\mathbf{h}}_{vu'}^l))) \\ \mathbf{h}_u^l &= \hat{\mathbf{h}}_u^l + \text{ReLU}(\text{GN}_{G_1 G_2}(\mathbf{W}_6^l \hat{\mathbf{h}}_u^l + \sum_{v' \in V_1} \mathbf{W}_7^l \hat{\mathbf{h}}_{v'}^l \odot \sigma(\tilde{\mathbf{h}}_{uv'}^l)))\end{aligned}\quad (11)$$

where $\mathbf{W}_1^l, \mathbf{W}_2^l, \mathbf{W}_3^l, \mathbf{W}_4^l, \mathbf{W}_5^l, \mathbf{W}_6^l, \mathbf{W}_7^l$ are learnable parameters at layer l , GN_π denote the graph normalization over all node pairs and $\text{GN}_{G_1 G_2}$ denote the graph normalization over all nodes in both graphs G_1 and G_2 .

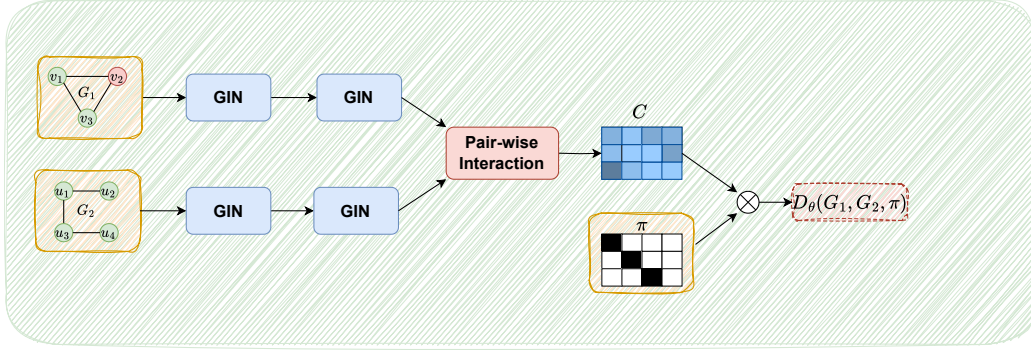
For a L -layer denoising network g_ϕ , the final matching score of each node pair is computed as follows:

$$g_\phi(G_1, G_2, \pi^t, t)[v][u] = \text{MLP}(\mathbf{h}_{vu}^L) + \text{MLP}(\mathbf{h}_{uv}^L) \quad (12)$$

Network Architecture of D_θ . The discriminator D_θ takes as input a graph pair (G_1, G_2) and a matching matrix π , then predicts a overall score for π . To better evaluate π , D_θ adopts the same structure as g_ϕ , which computes the embeddings of each node pair in π , and computes the overall score based on the pair embeddings. Specifically, computing the embeddings for each node pair enables D_θ to distinguish the influence of individual node pairs in π , while the use of AGNN allows D_θ to effectively capture complex dependencies between node pairs. An overview of D_θ 's network architecture is presented in Figure 5(a).



(a) Network architecture of D_θ in GEDRanker



(b) Network architecture of D_θ in GEDRanker (cost)

Figure 5: Comparison of D_θ 's network architecture.

However, since D_θ does not include the time step t as an input, we remove the time step component from AGNN of the second update stage as follows:

$$\begin{aligned}
 \hat{h}_{vu}^l &= W_1^l h_{vu}^{l-1}, \quad \hat{h}_{uv}^l = W_1^l h_{uv}^{l-1} \\
 \tilde{h}_{vu}^l &= W_2^l \hat{h}_{vu}^l + W_3^l \hat{h}_v^l + W_4^l \hat{h}_u^l \\
 \tilde{h}_{uv}^l &= W_2^l \hat{h}_{uv}^l + W_3^l \hat{h}_u^l + W_4^l \hat{h}_v^l \\
 h_{vu}^l &= \hat{h}_{vu}^l + \text{MLP}(\text{ReLU}(\text{GN}_\pi(\tilde{h}_{vu}^l))) \\
 h_{uv}^l &= \hat{h}_{uv}^l + \text{MLP}(\text{ReLU}(\text{GN}_\pi(\tilde{h}_{uv}^l))) \\
 h_v^l &= \hat{h}_v^l + \text{ReLU}(\text{GN}_{G_1 G_2}(W_6^l \hat{h}_v^l + \sum_{u' \in V_2} W_7^l \hat{h}_{u'}^l \odot \sigma(\tilde{h}_{vu'}^l))) \\
 h_u^l &= \hat{h}_u^l + \text{ReLU}(\text{GN}_{G_1 G_2}(W_6^l \hat{h}_u^l + \sum_{v' \in V_1} W_7^l \hat{h}_{v'}^l \odot \sigma(\tilde{h}_{uv'}^l)))
 \end{aligned} \tag{13}$$

For a L -layer discriminator D_θ , the overall score of π is computed as follows:

$$D_\theta(G_1, G_2, \pi) = \sum_{(v,u) \in \pi} (\text{MLP}(h_{vu}^L) + \text{MLP}(h_{uv}^L)) \tag{14}$$

A.4 Alternative Ranking Loss

Hinge Loss. Hinge loss could be an alternative ranking loss for our preference-aware discriminator. At each training step, for a pair of graphs, given the current best node matching matrix π and the

predicted $\hat{\pi}_{g_\phi}$, the discriminator can be trained to minimize the following Hinge loss:

$$\mathcal{L}_{Hinge}(\hat{\pi}_{g_\phi}, \bar{\pi}) = \begin{cases} \max(0, D_\theta(G_1, G_2, \bar{\pi}) - D_\theta(G_1, G_2, \hat{\pi}_{g_\phi}) + \text{margin}) & \text{if } c(G_1, G_2, \pi_{g_\phi}) \leq c(G_1, G_2, \bar{\pi}) \\ \max(0, D_\theta(G_1, G_2, \hat{\pi}_{g_\phi}) - D_\theta(G_1, G_2, \bar{\pi}) + \text{margin}) & \text{if } c(G_1, G_2, \pi_{g_\phi}) \geq c(G_1, G_2, \bar{\pi}) \end{cases} \quad (15)$$

where margin is set to 0 if $c(G_1, G_2, \pi_{g_\phi}) = c(G_1, G_2, \bar{\pi})$, otherwise 1.

B Experimental Setting

B.1 Dataset

We conduct experiments on three widely used real world datasets: AIDS700 [17], Linux [33, 17], and IMDB [17, 34]. Table 3 shows the statistics of the datasets. For each dataset, we split into 60%, 20% and 20% as training graphs, validation graphs and testing graphs, respectively.

To construct training graph pairs, all training graphs with no more than 10 nodes are paired with each other. For these small graph pairs, the ground-truth GEDs and node matching matrices are obtained using the exact algorithm. For graph pairs with more than 10 nodes, ground-truth labels are infeasible to obtain, we follow the strategy described in [11] to generate 100 synthetic graphs for each training graph with more than 10 nodes. Specifically, for a given graph, we apply Δ random edit operations to it, where Δ is randomly distributed in $[1, 10]$ for graphs with more than 20 nodes, and is randomly distributed in $[1, 5]$ for graphs with no more than 20 nodes. Δ is used as an approximation of the ground-truth GED.

To form the validation/testing graph pairs, each validation/testing graph with no more than 10 nodes is paired with 100 randomly selected training graphs with no more than 10 nodes. And each validation/testing graph with more than 10 nodes is paired with 100 synthetic graphs.

Table 3: Dataset statistics.

Dataset	# Graphs	Avg $ V $	Avg $ E $	Max $ V $	Max $ E $	Number of Labels
AIDS700	700	8.9	8.8	10	14	29
Linux	1000	7.6	6.9	10	13	1
IMDB	1500	13	65.9	89	1467	1

B.2 Implementation Details

Network. The denoising network g_ϕ consists of 6 layers with output dimensions $[128, 64, 32, 32, 32, 32]$, while the discriminator D_θ consists of 3 layers with output dimensions $[128, 64, 32]$.

Training. During training, the number of time steps T for the forward process is set to 1000 with a linear noise schedule, where $\beta_0 = 10^{-4}$ and $\beta_T = 0.02$. For the Gumbel-Sinkhorn operator, the number of iterations K is set to 5 and the temperature τ is set to 1. Moreover, we train g_ϕ and D_θ for 200 epochs with a batch size of 128. The loss weight λ for $\mathcal{L}_{\text{explore}}$ in \mathcal{L}_{g_ϕ} (Equation 6) is linearly annealed from 1 to 0 during the first 100 epochs, and fixed at 0 for the remaining 100 epochs. For the optimizer, We adopt RMSProp with a learning rate of 0.001 and a weight decay of 5×10^{-4} .

Inference. During inference, the number of time steps S for the reverse process is set to 10 with a linear denoising schedule. For each test graph pair, we generate $k = 100$ candidate node matching matrices in parallel.

Testbed. All experiments are performed using an NVIDIA GeForce RTX 3090 24GB and an Intel Core i9-12900K CPU with 128GB RAM.

Table 4: Overall performance on unseen testing graph pairs.

Datasets	Models	Type	MAE ↓	Accuracy ↑	ρ ↑	τ ↑	$p@10$ ↑	$p@20$ ↑	Time(s) ↓
AIDS700	Hungarian	Trad	8.237	1.5%	0.527	0.416	54.3%	60.3%	0.0001
	VJ	Trad	14.171	0.9%	0.391	0.302	44.9%	52.9%	0.00016
	GEDGW	Trad	0.828	53%	0.85	0.764	86.4%	85.8%	0.38911
	Noah	SL	3.174	6.8%	0.735	0.617	77.8%	76.4%	0.5765
	GENN-A*	SL	0.508	67.1%	0.917	0.836	87.1%	90.6%	3.44326
	MATA*	SL	0.885	56.6%	0.77	0.689	73.2%	76.6%	0.00486
	GEDGNN	SL	1.155	50.5%	0.838	0.746	89.1%	87.6%	0.39344
	GEDIOT	SL	1.348	47.4%	0.81	0.71	88.4%	86.9%	0.39707
	DiffGED	SL	0.024	96.4%	0.993	0.986	99.7%	99.7%	0.07546
	GEDRanker (Ours)	UL	0.101	91.4%	0.981	0.963	99%	99%	0.07616
Linux	Hungarian	Trad	5.423	7.5%	0.725	0.623	75%	77%	0.00008
	VJ	Trad	11.174	0.4%	0.613	0.512	70.6%	74.5%	0.00013
	GEDGW	Trad	0.568	73.5%	0.925	0.865	90.9%	91.5%	0.17768
	Noah	SL	1.879	8%	0.872	0.796	84.3%	92.2%	0.25712
	GENN-A*	SL	0.142	92.9%	0.976	0.94	99.6%	99.6%	1.17702
	MATA*	SL	0.201	91.5%	0.948	0.903	86.2%	90.2%	0.00464
	GEDGNN	SL	0.105	96.2%	0.979	0.968	98.6%	98.5%	0.12169
	GEDIOT	SL	0.14	94.8%	0.973	0.959	98.1%	98.3%	0.12826
	DiffGED	SL	0.0	100%	1.0	1.0	100%	100%	0.06901
	GEDRanker (Ours)	UL	0.008	99.6%	0.998	0.997	99.5%	99.7%	0.07065
IMDB	Hungarian	Trad	21.156	45.9%	0.776	0.717	84.2%	82.1%	0.00012
	VJ	Trad	44.072	26.6%	0.4	0.359	60.1%	63.1%	0.00037
	GEDGW	Trad	0.349	93.9%	0.966	0.953	99.2%	98.3%	0.37384
	Noah	SL	-	-	-	-	-	-	-
	GENN-A*	SL	-	-	-	-	-	-	-
	MATA*	SL	-	-	-	-	-	-	-
	GEDGNN	SL	2.484	85.5%	0.895	0.876	92.3%	91.7%	0.42662
	GEDIOT	SL	2.83	84.4%	0.989	0.876	92.5%	92.4%	0.42269
	DiffGED	SL	0.932	94.6%	0.982	0.974	97.5%	98.4%	0.15107
	GEDRanker (Ours)	UL	1.025	93.9%	0.998	0.968	96%	97%	0.15012

C More Experimental Results

C.1 Generalization Ability

To evaluate the generalization ability of GEDRanker, we construct testing graph pairs by pairing each testing graph with 100 unseen testing graphs, instead of with training graphs. The overall performance on these unseen pairs is reported in Table 4. On unseen testing pairs, our unsupervised GEDRanker continues to achieve near-optimal performance, with only a marginal gap compared to the supervised DiffGED, and consistently outperforms all other supervised and traditional baselines. Furthermore, compared to the results in Table 1, there is no significant performance drop, demonstrating the generalization ability of our GEDRanker.

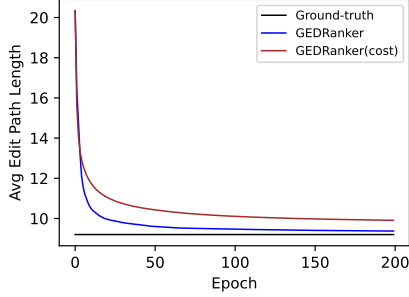
C.2 Scalability

Table 5: Overall performance on large testing graph pairs.

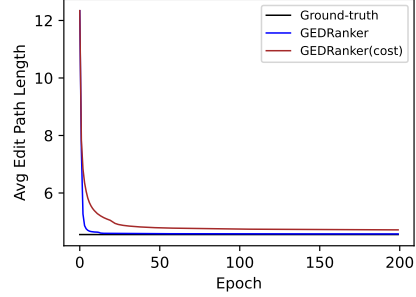
Datasets	Models	Average GED ↓	Time(s) ↓
IMDB-large	Hungarian	234.656	0.00016
	VJ	219.465	0.00039
	GEDGW	140.278	0.4032
	GEDRanker (Ours)	140.138	0.1904

Table 6: Ablation study on D_θ 's network architecture.

Datasets	Models	MAE ↓	Accuracy ↑	ρ ↑	τ ↑	$p@10$ ↑	$p@20$ ↑
AIDS700	GEDRanker (cost)	0.528	66.3%	0.907	0.841	90.4%	92%
	GEDRanker	0.088	92.6%	0.984	0.969	99.1%	99.1%
Linux	GEDRanker (cost)	0.102	94.9%	0.98	0.965	96.8%	97.1%
	GEDRanker	0.01	99.5%	0.997	0.995	100%	99.8%



(a) AIDS700



(b) Linux

Figure 6: Impact of D_θ 's network architecture on the average edit path length of the best found node matching matrices on training graph pairs.

To further evaluate the scalability of GEDRanker, we construct training pairs by pairing each large training graph in the IMDB dataset with all other large training graphs, instead of using synthetic graphs. For testing, we form pairs by pairing each large testing graph with 100 large training graphs. Since ground-truth labels are unavailable for large graph pairs, all supervised learning methods cannot be trained, we compare GEDRanker only against traditional baseline methods. We report the average estimated GED across all testing pairs, along with the average inference time per testing pair.

Table 5 summarizes the overall performance of GEDRanker and traditional baseline methods on the large IMDB testing graph pairs. GEDRanker achieves the lowest average estimated GED, and compared to GEDGW, GEDRanker offers significantly faster inference, highlighting its scalability.

C.3 Ablation Study on the Network Architecture of D_θ

To evaluate the impact of D_θ 's network architecture on the performance of GEDRanker, we create a variant model, *GEDRanker (cost)*, that adopts an alternative network design inspired by typical architectures used in regression-based GED estimation [11, 12]. Figure 5(b) shows an overview of the network architecture of D_θ in GEDRanker (cost).

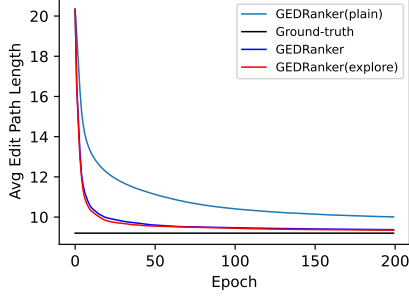
Specifically, given a graph pair (G_1, G_2) and a node matching matrix π , we compute nodes embeddings using GIN. Based on the pairwise node interactions, we then construct a matching cost matrix $C \in \mathbb{R}^{|V_1| \times |V_2|}$. Finally, the score $D_\theta(G_1, G_2, \pi)$ is estimated by $\langle \pi, C \rangle$. The overall architecture of D_θ can be represented as follows:

$$\begin{aligned}
h_v^l &= \text{GN}_{G_1}(\text{MLP}((1 + \epsilon^l) \cdot h_v^{l-1} + \sum_{v' \in \mathcal{N}_{G_1}(v)} h_{v'}^{l-1})) \\
h_u^l &= \text{GN}_{G_2}(\text{MLP}((1 + \epsilon^l) \cdot h_u^{l-1} + \sum_{u' \in \mathcal{N}_{G_2}(u)} h_{u'}^{l-1})) \\
H_1 &= [h_v^L]_{v \in V_1}, \quad H_2 = [h_u^L]_{u \in V_2} \\
C &= \text{MLP}([H_1 W_1 H_2^\top, H_1 W_2 H_2^\top, \dots, H_1 W_n H_2^\top]) \\
D_\theta(G_1, G_2, \pi) &= \langle \pi, C \rangle
\end{aligned} \tag{16}$$

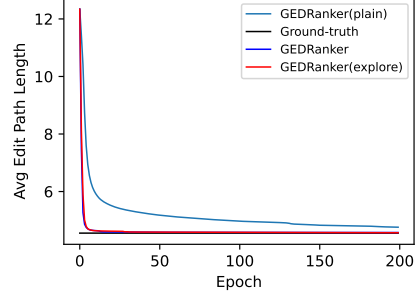
where we set $L = 3$ and $n = 16$.

Table 7: Ablation study on loss weight λ .

Datasets	Models	MAE \downarrow	Accuracy \uparrow	$\rho \uparrow$	$\tau \uparrow$	$p@10 \uparrow$	$p@20 \uparrow$
AIDS700	GEDRanker (plain)	0.549	65.4%	0.905	0.837	91.7%	91.5%
	GEDRanker (explore)	1.334	39.3%	0.789	0.689	76.5%	79.9%
	GEDRanker	0.088	92.6%	0.984	0.969	99.1%	99.1%
Linux	GEDRanker (plain)	0.079	96.2%	0.984	0.973	98.1%	98.3%
	GEDRanker (explore)	0.146	93.4%	0.973	0.955	96.6%	98.2%
	GEDRanker	0.01	99.5%	0.997	0.995	100%	99.8%



(a) AIDS700



(b) Linux

Figure 7: Impact of λ 's network architecture on the average edit path length of the best found node matching matrices on training graph pairs.

Table 6 shows the overall performance of GEDRanker (cost). Surprisingly, GEDRanker (cost) performs significantly worse than GEDRanker. This phenomenon can be attributed to the following reasons: (1) Although GEDRanker (cost) estimates the score by assigning each node pair in π an individual cost from C , these costs are fixed for each node pair, irrespective of the actual value in π . The final score is computed as a simple linear combination $\langle \pi, C \rangle$, which neglects the complex dependencies and interactions among node pairs. In contrast, D_θ in our GEDRanker directly computes node pair embeddings conditioned on the value in π , and leverages AGNN to capture interactions among node pairs; (2) The node matching matrix π is inherently sparse, with most of its elements being 0. This sparsity significantly limits the ability of D_θ to learn correct C as only a few nonzero elements contribute to gradient updates. In contrast, D_θ in our GEDRanker transforms each value in π into embeddings that enables effective gradient updates even the value is 0 in π .

Consequently, D_θ in GEDRanker (cost) struggles to estimate the correct preference order over different π , thereby misguiding g_ϕ 's exploration direction, as demonstrated in Figure 6. This ultimately results in inferior performance.

C.4 Ablation Study on Loss Weight λ

In our GEDRanker, g_ϕ is trained to minimize $\mathcal{L}_{g_\phi} = \mathcal{L}_{rec(\bar{\pi})} + \lambda \mathcal{L}_{explore}$, where the loss weight λ is dynamically annealed during training to prioritize exploration in the early stages and shift g_ϕ 's focus toward recovering high-quality (exploitation) in the later stages. In Section 5.3, we evaluated GEDRanker (plain), which trains g_ϕ without any exploration by setting $\lambda = 0$. To understand the impact of prioritizing exploration through the entire training process, we create a variant model, *GEDRanker (explore)*, where λ is fixed at 1.

Table 7 compares the performance of GEDRanker under different settings of λ . It is unexpected to observe that GEDRanker (explore) performs extremely poorly on the AIDS700 dataset. Although GEDRanker (explore) demonstrates strong exploration ability comparable to GEDRanker, as illustrated in Figure 7, its performance is still significantly worse.

The reason for this phenomenon lies in the mismatch between the training objective and the reverse diffusion process during inference. In a standard diffusion model, the reverse process is designed to gradually remove noise from the noisy node matching matrix step by step through a Markov chain

(see Equation 2). During this process, g_ϕ is expected to correctly remove the noise from π^t . However, GEDRanker (explore) prioritizes exploration throughout the entire training process. This excessive focus on exploration prevents g_ϕ from learning the essential noise-removal patterns required by the reverse process. Although g_ϕ might still output high-quality node matching probability matrices at some steps, it still disrupts the reverse diffusion path, causing significant misalignment with the expected denoising trajectory. Consequently, errors are accumulated during reverse process, leading to inferior performance.

In contrast, our GEDRanker dynamically decreases λ during training, promoting strong exploration in the early stages, while gradually shifting focus toward effective denoising of π^t in alignment with the reverse diffusion process. This balanced strategy enables both thorough exploration during training and high-quality solutions during inference.